Research Article

Photocurrent generation through peptide-based self-assembled monolayers on a gold surface: antenna and junction effects[‡][§]

Emanuela Gatto,[a] Mario Caruso,[a] Alessandro Porchetta,[a] Claudio Toniolo,[b] Fernando Formaggio,[b] Marco Crisma[b] and Mariano Venanzi[a]*

The photocurrent generation properties of mono- and bi-component peptide-based self-assembled monolayers (SAMs) immobilized on a gold surface were studied by electrochemical and spectroscopic techniques. The peptides investigated comprised almost exclusively C^α-tetrasubstituted α-amino acids. These non-coded residues, because of their unique conformational properties, forced the peptide backbone to attain a helical conformation, as confirmed by X-ray crystal structure and CD determinations in solution. The peptide helical structure promoted the formation of a stable SAM on the gold surface, characterized by an electric macrodipole directed from the $C(\delta^-)$ to the $N(\delta^+)$ terminus, that remarkably affected the electron transfer (ET) process through the peptide chain. The peptides investigated were derivatized with chromophores strongly absorbing in the UV region to enhance the efficiency of the photocurrent generation (*antenna effect*). The influence of the nature of the peptide–gold interface on the ET process (*junction effect*) was analyzed by comparing the photocurrent generation process in peptide SAMs immobilized on a gold surface through Au–S linkages with that in a bi-component SAM embedding a photoactive peptide into the linked palisade formed by disulfide-functionalized peptides. Copyright © 2010 European Peptide Society and John Wiley & Sons, Ltd.

Supporting information may be found in the online version of this article

Introduction

Self-assembly, i.e. the spontaneous organization of molecular building blocks to generate a supramolecular architecture, is the most promising approach for the construction of controlled nanometric structures [1–3]. This strategy has been leading to important results in several fields, providing new-concept smart materials for tissue engineering, controlled drug release, nucleic acid and protein sensing, organic photovoltaics and molecular electronics [4–6]. More specifically, in microelectronics the capability to produce smaller structures allows for location of more components in the same space, faster operations, and lower power consumption [7].

Biomolecules have been extensively investigated as possible components of nano-scaled electronic devices [8]. In particular, hybrid materials obtained by functionalizing metals or semiconductors with biomolecules or bioinspired molecular systems have been recently synthesized, paving the way for the fast-growing field of bioelectronics [9]. In this regard, one of the major issues to be faced is the control of the structure and morphology of the biolayer when immobilized on an inorganic support. This goal, particularly relevant for preserving the activity of the biomolecule and obtaining regularly patterned domains as well, is a strict requirement for the addressability, storage and transmission of I/O signals. The most straightforward approach to the problem seems to govern the morphology of the grown mesoscopic structure at the level of the conformational properties of the single building-block element.

Sophisticated strategies have been developed to synthesize amino acids with particular conformational properties, aiming to obtain peptide foldamers, i.e. peptides able to attain specific secondary structures [10]. In particular, peptides rich in C^α-tetrasubstituted residues have been found to overwhelmingly populate helically ordered structures, the exact geometry of which can be controlled by properly selecting the amino acid constituents [11,12]. Short peptides rich in the achiral α-aminoisobutyric acid (Aib) are well known to adopt preferentially
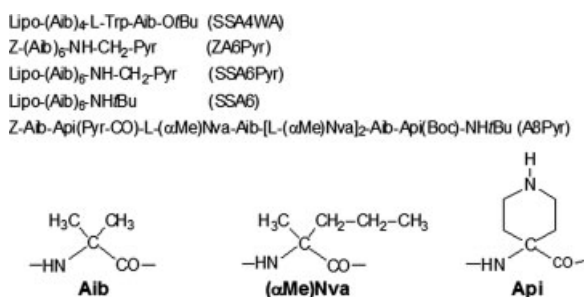
* Correspondence to: *Mariano Venanzi, Department of Chemical Sciences and Technologies, University of Rome "Tor Vergata", 00133 Rome, Italy. E-mail: venanzi@uniroma2.it*

a *Department of Chemical Sciences and Technologies, University of Rome "Tor Vergata", 00133 Rome, Italy*

b *ICB, Padova Unit, CNR, Department of Chemistry, University of Padova, 35131 Padova, Italy*

Figure 1. Primary structures and acronyms of the peptides investigated. All the peptides are exclusively formed by C^α-tetrasubstituted α-amino acids, the chemical structures of which are also shown (bottom). Lipo, (S,R)-lipoyl; Aib, α-aminoisobutyric acid; OtBu, tert-butoxy; Z, benzyloxycarbonyl; Pyr, 1-pyrenyl; NHtBu, tert-butylamino; Api, 4-aminopiperidine-4-carboxylic acid; (αMe)Nva, C^α-methylnorvaline; Boc, tert-butyloxycarbonyl.

the 3_{10}-helix conformation ($\varphi = \pm57°$, $\psi = \pm30°$) [13]. Most interestingly, helical peptides have shown superior electron transfer (ET) efficiencies in terms of rate constant values, long-range character and directional asymmetry of the ET process [14]. In this connection, an important feature of helical peptides is the electrostatic field generated by the macrodipole resulting from the vector sum of the electric dipoles associated with the peptide bond of each residue (3.5 D per residue) [15–17]. This property endows a self-assembled monolayer (SAM) formed by helical peptides with a specific polarity, the negative end being positioned at the $C(\delta-)$- and the positive head at the $N(\delta+)$-terminus. It has been shown that such an electrostatic field significantly affects the efficiency and the direction of the ET process through the peptide chain, stabilizing the charge-transfer state properly aligned along the field [18–20]. It should be also noted that, in the formation of a peptide SAM, helical peptides functionalized by a thiol group at the N-terminus are preferentially bound to the gold surface with respect to C-terminated thio-peptides, because in the former compounds the $Au^{\delta+}–S^{\delta-}$ bond is stabilized by the electrostatic effect exerted by the helix macrodipole [16,21].

We have recently shown that a hexapeptide, comprising five Aib residues, one Trp positioned near the C-terminus, and a lipo group at the N-terminus, formed a densely packed SAM on a gold surface, with interesting growth dynamics and self-healing properties [21]. Owing to the high content of Aib residues, this peptide, denoted in the following as SSA4WA (Figure 1), was shown to adopt a 3_{10}-helix conformation in solution. The morphology of the SAM formed by SSA4WA was characterized by quartz crystal microbalance, infrared reflectance anisotropy and scanning tunneling microscopy [22,23]. Very recently, we have reported that SSA4WA gives rise to a net photocurrent when excited with UV radiation, due to the absorption properties of Trp in this spectral region (antenna effect) [24].

In the present work, we investigated the photocurrent generation properties of two new peptide foldamers, SSA6Pyr and A8Pyr (Figure 1), formed exclusively by C^α-tetrasubstituted α-amino acids and both functionalized with a Pyr antenna group, positioned at the C- and in the proximity of the N-terminus, respectively. Pyr was selected for its stronger absorption features at longer wavelengths with respect to those of the indole chromophore of Trp and for its particular emission properties, extremely sensitive to the onset of Pyr–Pyr interactions (excimer formation) [25]. The Pyr absorption properties allowed us to perform photocurrent experiments minimizing the direct emission of photoexcited electrons from the gold surface, which starts be-

coming important at excitation wavelengths shorter than 260 nm ($\sim$5 eV). SSA6Pyr was functionalized with a lipo group at the N-terminus for binding to gold, while A8Pyr, lacking the lipo or other S-containing groups, cannot exploit the Au–S great affinity for stable immobilization on gold. An Aib homo-hexapeptide (SSA6, Figure 1), also functionalized at the N-terminus with a lipo group but with the Pyr chromophore missing, was also prepared as a reference compound.

The photocurrent generation properties of mono- and bi-component SAMs formed by these peptides have been studied by electrochemical and spectroscopic techniques, focusing on the antenna effect produced by the chromophores covalently linked to the peptide chain. The photocurrent generation efficiency was also found to strongly depend on the intimate structure of the peptide–gold interface, characterized by the strong Au–S linkage ($\sim$40 kcal·mol^{-1}) for the lipo-substituted peptides (SSA4WA and SSA6Pyr) and by physically adsorbed photoactive peptides in the case of the bi-component SAMs formed by A8Pyr, entrapped into the Au–S-linked monolayer assembled by SSA4WA or SSA6 (junction effect).

Materials and Methods

Materials

The synthesis and chemical and conformational characterizations of the peptides SSA4WA, Z-A6Pyr, SSA6Pyr, SSA6 and A8Pyr were reported elsewhere [20–22,24,26,27]. Spectrograde solvents (Carlo Erba, Milan, Italy) were exclusively used. Water was distilled and passed through a Milli-Q purification system. Other chemicals, triethanolamine (TEOA) (Fluka, Buchs, Switzerland), potassium chloride, sodium sulphate (Carlo Erba, Milan, Italy), potassium ferricyanide, methylviologen and undecanethiol (Aldrich, Buchs, Switzerland) were all of reagent grade quality and used without further purification.

Preparation of Self-assembled Peptide Thin Films

Gold electrodes were etched for 15 min in a freshly prepared piranha solution (2:1 sulphuric acid/H_2O_2, v/v), rinsed with bi-distilled water and ethanol (5 min each) before immersion in the peptide solution for the SAM deposition. SAM-coated electrodes were prepared by dipping a gold electrode into an 1 mM ethanol solution of the peptide in a N_2 atmosphere. After 18 h, the electrode was repeatedly rinsed (five times) with ethanol to remove physically adsorbed peptides from the SAM and dried for 3 min under a gentle argon flow. The surface covering of the peptide film was estimated by cyclic voltammetry (CV) measurements in NaOH 0.5 M, integrating the irreversible reduction peak of Au–S linkage (-0.9 V) [28]. In all cases we found a value slightly higher than that theoretically evaluated for an electrode surface fully covered by hexagonally packed 3_{10}-helix peptide chains tilted by 0° with respect to the vertical to the surface (2.7×10^{-10} mol·cm^{-2}). This clearly results from the underestimation of the real electrode surface, because only the geometrical electrode surface was taken into account in the theoretical assessment. Bi-component peptide SAMs were prepared by mixing two 0.5 mM ethanol–water 3:1 v/v solutions of the two peptides. Deposition time and rinsing procedures were the same as those used for the preparation of the single-component SAM. Water was added to favor the formation of the peptide SAM by hydrophobic effect. The reported relative compositions of the bi-component SAMs were those (v/v) of the original deposition solution.

Methods

Electrochemistry

Cyclic voltammograms were obtained by using a PG-310 potentiostat (Heka Elektronik). CV experiments were carried out at room temperature, adopting a standard three-electrode configuration with a SAM-coated gold electrode as the working electrode, a platinum wire as the auxiliary electrode and Ag/AgCl as the reference electrode. Blocking experiments were carried out with a 0.5 mM $K_3Fe(CN)_6$ solution in 1 M KCl at a sweep rate of 50 mV·s^{-1}. Photocurrent measurements were carried out at room temperature using the three-electrode set-up described above, by using Na_2SO_4 (0.1 M) as the supporting electrolyte and TEOA at 50 mM concentration acting as electron donor in solution. In this experiment, the SAM-modified electrode was irradiated with a Xe lamp (150 W) equipped with a monochromator and the generated photocurrent was detected by the voltammetric analyzer described above. The incident photon-to-current efficiency (IPCE) has been determined by using the following equation [29]:

$$IPCE(\%) = \frac{100i(A/\text{cm}^2)1240}{I(W/\text{cm}^2)\lambda(\text{nm})}$$

where i is the measured photocurrent, I is the incident light power density, and λ is the incident wavelength (340 nm). The intensity of the incident light was evaluated by azobenzene actinometry [30].

X-ray diffraction

Single crystals of Z-A6Pyr sesquihydrate were grown by slow evaporation from a methanol solution. Diffraction data were collected on a Philips PW1100 four-circle diffractometer, using graphite-monochromated CuKα radiation. Unit cell parameters were obtained by least-squares refinement of the angular settings of 48 carefully centered reflections in the 12–18° θ range. Intensities were corrected for Lorentz and polarization effects, not for absorption. The structure was solved by direct methods of the SIR 2002 program [31]. Refinement was carried out by full-matrix least-squares on F^2, using all data, by application of the SHELXL-97 program [32], with all non-H-atoms anisotropic. H-atoms of the peptide molecule were calculated at idealized positions and refined using a riding model. The positions of both H-atoms bonded to the co-crystallized O1W water molecule and one bonded to O2W were located on a difference Fourier map and were not refined.

Circular dichroism (CD) and Fluorescence

CD experiments in solution were carried out by a Jasco J-600 spectropolarimeter using quartz cuvettes ($l = 0.1, 0.5, 1$ cm). Steady-state fluorescence experiments were carried out on a Fluoromax spectrofluorimeter (Jobin-Yvon) operating in the single-photon counting mode. For the fluorescence measurements, the peptide SAMs were immobilized on a transparent glass coated with a 5-nm thick Au layer. The glass was mounted on a solid sample holder and the signal detected at 45° for minimizing any scattered light contamination.

Results and Discussion

X-ray Diffraction and Circular Dichroism

The high tendency of oligopeptides formed by C^α-tetrasubstituted residues to fold in a helical structure was confirmed by
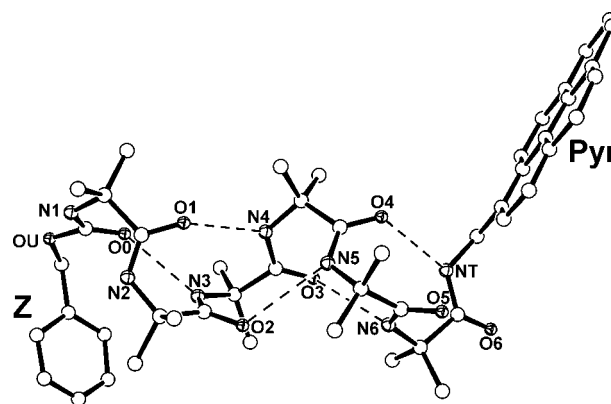

Figure 2. X-ray diffraction structure of Z-(Aib)$_6$-NH-CH$_2$-Pyr with partial atom numbering. The five intramolecular C=O–H–N H-bonds are indicated by dashed lines. The $i \leftarrow i+3$ pattern of intramolecular H-bonds, characteristic of the 3$_{10}$-helix conformation, can be clearly recognized.

X-ray diffraction measurements on the Z-synthetic precursor of SSA6Pyr (Z-A6Pyr). The 3$_{10}$-helix conformation attained by Z-A6Pyr in the crystal state is clearly recognized in the 3D-structure reported in Figure 2, where the characteristic $i \leftarrow i + 3$ pattern of intramolecular H-bonds can be easily observed. Crystal data, structure refinement information, selected values of the torsion angles and geometric parameters of intra- and intermolecular H-bonds were reported in Tables S1–S3 (see Supporting Information). The CD spectrum of A8Pyr in acetonitrile (Figure S1, Supporting Information) shows a strong negative maximum at 208 nm and a weak negative shoulder at 225 nm, indicating that the 3$_{10}$-helix conformation [33] is also predominantly populated in solution.

Cyclic Voltammetry

CV (blocking) experiments carried out on gold electrodes coated with a peptide SAM gave basic information on the stability and packing density of the peptide layer on the electroactive surface. From the CV curves reported in Figure 3, it can be easily seen that, for all of the peptide SAMs investigated, the discharge of ferricyanide was depleted by the immobilization of the peptide layer on the gold electrode. However, from a close inspection of the results shown in Figure 3(A), it appears that the SSA6Pyr SAM is characterized by a higher blocking capacity with respect to the SSA6 SAM, suggesting that Pyr–Pyr interactions may contribute to stabilize the peptide layer. Figure 3(B) reported the CV curves measured for the 1:10 SSA6Pyr/SSA6 and 1:1 SSA6Pyr/SSA4WA bi-component SAMs. It is worth noting that while for the former SAM the CV results indicate a residual activity of the electrolyte in solution, for the latter the electrolyte discharge is almost completely inhibited, suggesting that also in this case aromatic–aromatic, i.e. Pyr–Trp interactions, may contribute to stabilize the bi-component SAM.

A different approach has been used for the formation of a bi-component SAM, composed of SSA4WA, covalently linked to the gold surface through Au–S interaction, and A8Pyr, tethered into the SSA4WA palisade. It was shown that a bi-component SAM formed by two helical peptides linked to a gold surface by an *N*-terminal and a *C*-terminal lipo group, respectively, was stabilized by the antiparallel arrangement of the two peptide chains by means of favorable inter-helical dipole–dipole interactions [34]. This effect was principally ascribed to the electric macrodipole
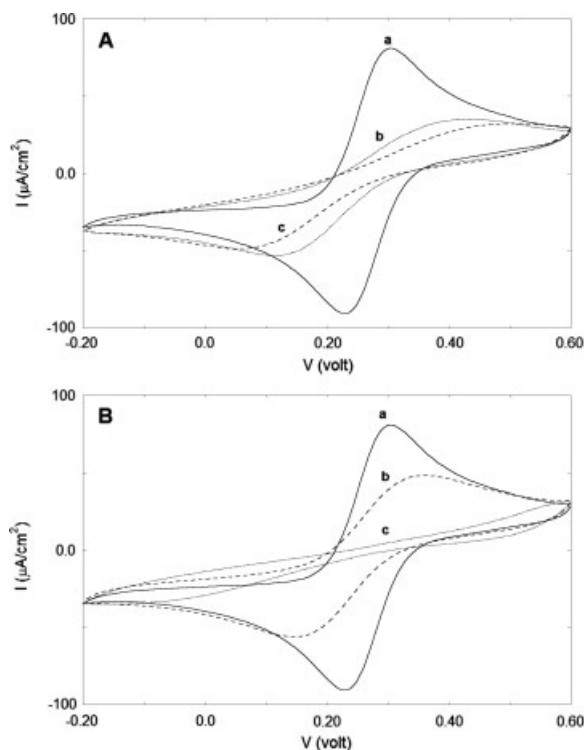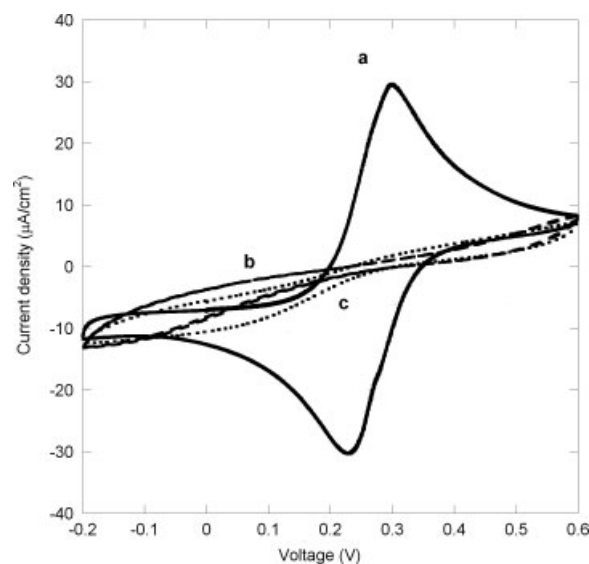
Figure 3. Cyclic voltammetry experiments in a 0.50 mM $K_3[Fe(CN)_6]$ aqueous solution for gold electrodes modified by the deposition of lipo-substituted peptide SAMs. The electrolyte discharge is inhibited by the formation of a densely packed peptide film. Working electrode: (A) bare gold (a, full line), gold electrode modified by SSA6 (b, dotted line) or SSA6Pyr (c, dashed line) SAMs; (B) bare gold (a, full line), gold electrode modified by 1:10 SSA6Pyr/SSA6 (b, dashed line) or 1:1 SSA6Pyr/SSA4WA (c, dotted line) SAMs. Sweep rate: 50 mV/s.

Figure 4. Cyclic voltammetry experiments in a 0.50 mM $K_3[Fe(CN)_6]$ aqueous solution for gold electrodes modified by the deposition of mono- (SSA4WA) and bi-component (A8Pyr/SSA4WA) peptide SAMs. The inclusion of A8Pyr in the SSA4WA SAM did not affect its packing density. Working electrode: bare gold (a, full line); gold electrode modified by SSA4WA (b, dashed line) or 1:1 A8Pyr/SSA4WA (c, dotted line) SAMs. Sweep rate: 50 mV/s.

associated with the peptide helical structure. In our case, the antiparallel arrangement of the two peptide foldamers (indeed SSA4WA has necessarily its positive end dipole directed toward the gold surface) favors the insertion of A8Pyr with its helix dipole positive end pointing toward the SAM outer surface. Importantly, in this arrangement both the Pyr and Trp chromophores would be located at the outer surface of the SAM and in contact with the electrolyte solution.

CV experiments carried out on a gold electrode modified by a A8Pyr/SSA4WA SAM in an aqueous $K_3Fe(CN)_6$ solution showed that the electrolyte discharge at the electrode is almost completely inhibited, indicating the dense packing of the bi-component SAM on the gold surface. The CV curves measured for the SSA4WA and A8Pyr/SSA4WA SAMs are reported in Figure 4 for comparison. The obvious conclusion is that the inclusion of A8Pyr in the SSA4WA SAM did not affect its packing density.

Steady-state Fluorescence

The fluorescence emission spectra of mono- and bi-component peptide SAMs were measured on glass supports coated with a 5-nm thick gold layer. In particular, the emission of the pyrene fluorescent probe in the SAMs formed by SSA6Pyr and A8Pyr was carefully investigated, focusing on the possible contribution of excimer-like emission. Pyr is a spatially sensitive fluorescent probe, which forms excited-state dimers (excimers) upon close encounter with another Pyr-based molecule [25]. Therefore, the observation of excimer emission signals the onset of close range
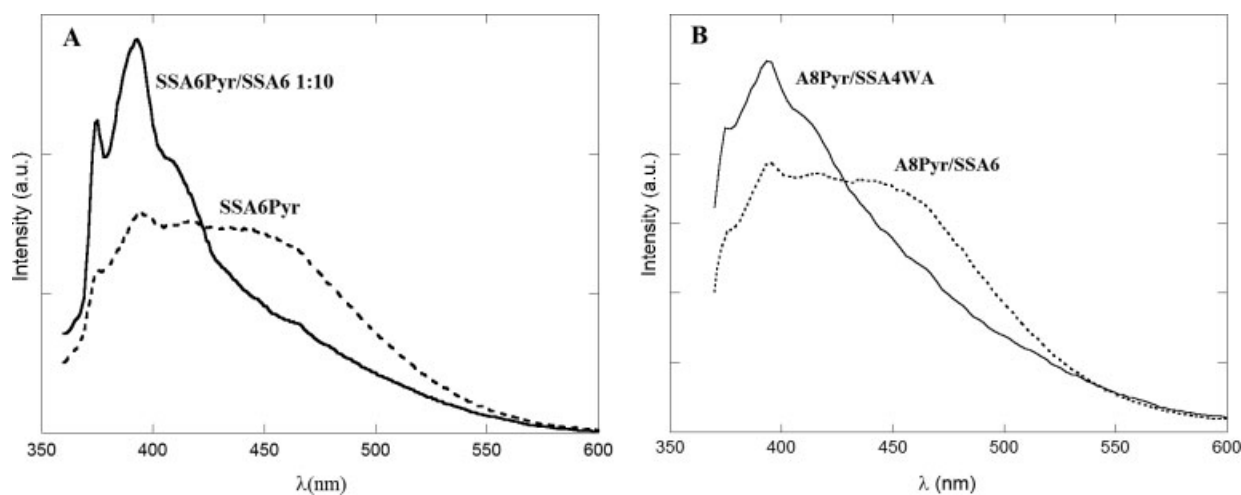
Pyr–Pyr interactions in the peptide SAMs, and, in case of a bi-component SAM, the formation of raft domains, i.e. segregated single-component regions. Formation of Pyr–Pyr excimers has been already observed in organic SAMs adsorbed on glass [35] or gold substrates [36], showing high emissive fluorescent properties and long-lived charge-transfer states.

In Figure 5(A), the emission spectra of the SAMs formed by SSA6Pyr and 1:10 SSA6Pyr/SSA6 are reported. While the fluorescence spectrum of the latter is typical of the Pyr monomer emission, in the former a strong contribution from fluorescent excimer species can be detected, which indicate a significant Pyr–Pyr excited-state interaction. This result parallels the CV evidence of a densely packed SAM in the case of SSA6Pyr and further supports the view that Pyr–Pyr interactions do stabilize the peptide SAM. It is also interesting to compare the emission spectra measured for the 1:1 A8Pyr/SSA4WA and the 1:1 A8Pyr/SSA6 bi-component SAMs (Figure 5(B)). The former emission spectrum is characteristic of a Pyr monomer emission, suggesting that A8Pyr and SSA4WA should be homogeneously intercalated in the bi-component SAM. In our view, A8Pyr, embedded in the defects of the SSA4WA palisade, gives rise to a densely packed SAM, as clearly shown by the CV results (Figure 4). On the other hand, the emission spectrum of the A8Pyr/SSA6 SAM revealed a significant contribution of excimer-like species. In this case, the relatively free dynamics of A8Pyr in the less organized SAM formed by SSA6 (Figure 3(A)) most likely allowed for the formation of local domains rich in A8Pyr. Thus, our fluorescence experiments, besides confirming the inclusion of A8Pyr in both the SSA4WA and SSA6 SAMs, nicely parallel the CV results and confirm the formation of a densely packed A8Pyr/SSA4WA SAM.

Photocurrent Generation

Despite intense research efforts, the importance of competitive mechanisms governing ET across peptide matrices is still strongly

Figure 5. Fluorescence emission spectra of single- and bi-component peptide SAMs functionalized with a Pyrene chromophore on gold coated glasses. The excimer emission signals the onset of Pyr–Pyr interactions. (A) 1 : 10 SSA6Pyr/SSA6 (full line); SSA6Pyr (dotted line). (B) 1 : 1 A8Pyr/SSA4WA (full line); 1 : 1 A8Pyr/SSA6 (dotted line). All the spectra are normalized to unit area.
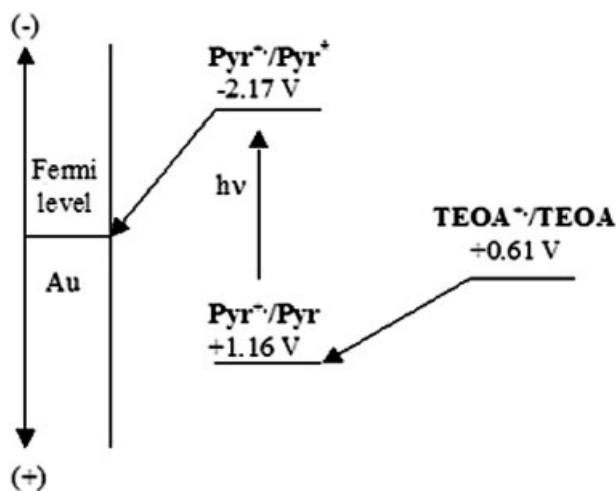
debated [14,37]. In the super-exchange model, the peptide chain mediates the coupling between the donor and the acceptor pair through electronic virtual states, while in the alternative hopping mechanism the electron jumps through the single amino acid residues with a finite time of residence on each bridging unit. The peptide bond has been proposed as the site of residence of the transferred electron, and the role of aromatic side chains as electron sink was recently unequivocally demonstrated [38]. Both mechanisms are thought to be operative (and to compete as well) at all distances. However, for short peptides ($n \leq 10$) and donor–acceptor distances less than 20 Å, the super-exchange mechanism was shown to predominate [39]. The overwhelming majority of these studies were carried out in solution on peptides functionalized with an ET donor–acceptor pair. The knowledge of ET or photoinduced ET through peptide chains in organic/inorganic hybrid systems is currently less clearly established, due to the complexity of the occurring physical processes and the relative paucity of experimental data. Photocurrent generation experiments through peptide SAMs have been actively investigated by Kimura and coworkers [16,40–45] who focused on the dependence of the ET efficiency on the peptide length, type of secondary structure, pH, role of aromatic residues, electronic coupling through the amino acid bridging units.

In this study, gold electrodes modified by the covalent deposition of mono- or bi-component peptide SAMs were employed as the working electrodes for photocurrent generation experiments in the UV–Vis absorption region. The current generated after photo-irradiation of the SAM formed by SSA6Pyr at different wavelengths in the presence of an electron donor in solution (i.e. TEOA) is shown in Figure 6, where the almost instantaneous rise and fall of the electronic current following the on/off switch of illumination can be appreciated. The IPCE for the SSA6Pyr SAM at $\lambda = 340$ nm was found to be equal to 0.05%. In this experiment, the Pyr chromophore, upon photoexcitation, gives rise to ET from its excited singlet state to the surface Fermi level of the gold electrode across the peptide spacer. This initial step is followed by a second ET event from TEOA to the Pyr radical cation, resulting in a net anodic current. In the final step, the reduction of the TEOA radical cation allows for closing the circuit. The processes taking place at the anode electrode are
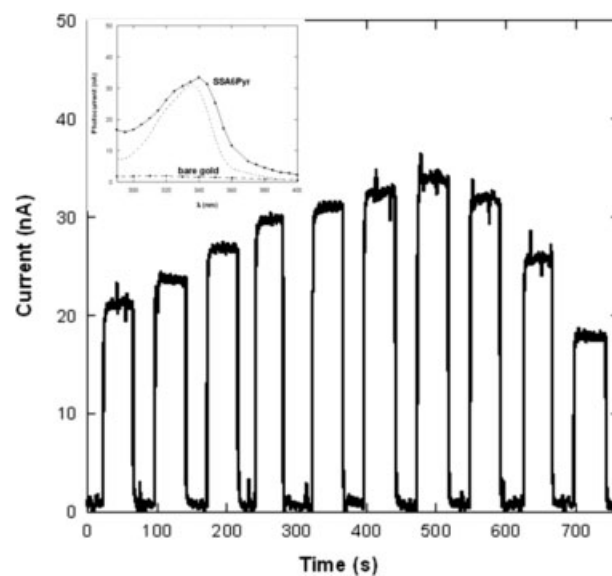
Figure 6. On/off cycles of electronic current upon photoexcitation of the Pyr unit in SSA6Pyr at different excitation wavelengths ($\lambda_{max} = 340$ nm). The electronic current intensities depend on the Pyr absorption spectrum, as shown by the excitation spectrum of SSA6Pyr reported in the inset. Inset: Photocurrent action spectrum and excitation spectrum of SSA6Pyr in the same experimental conditions (slit width = 15 nm). For comparison, the photocurrent action spectrum of the bare gold electrode is also reported.

diagrammatically sketched in Figure 7. The action spectrum, i.e. the excitation wavelength dependence of the measured photocurrent intensity, closely overlaps the Pyr absorption spectrum recorded under the same conditions (slit opening = 15 nm), thus confirming the identity of the photosensitizing species, as shown in the inset of Figure 6. The photoemission of a bare gold electrode under the same conditions (wavelength region, radiance and applied voltage) is negligible, as shown by the associated photocurrent action spectrum reported in the inset of Figure 6. The photocurrent action spectra of the SAMs formed by SSA6Pyr, 1 : 10 SSA6Pyr/SSA6, 1 : 1 A8Pyr/SSA4WA and A8Pyr/SSA6 in the Pyr absorption region are shown in Figure 8(A) and (B). The antenna effect of the Pyr chromophore is emphasized by the weak photocurrent measured
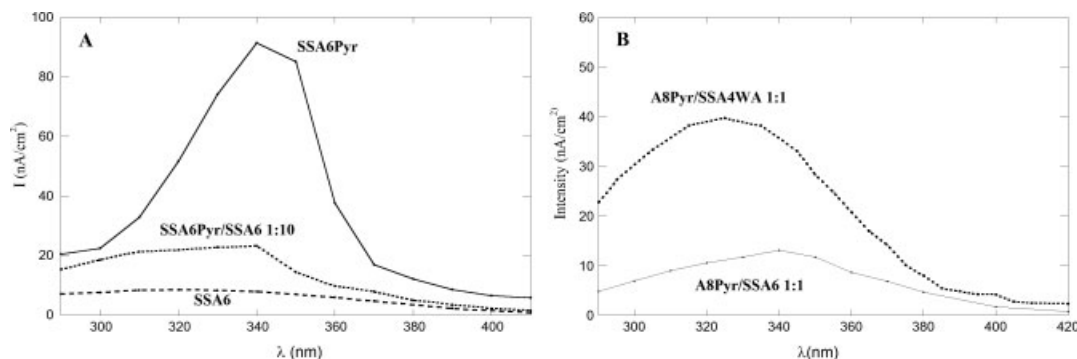
Figure 7. Sketch of the energetics and of the elementary processes triggered by photoexcitation of Pyr occurring at the gold electrode in anodic conditions (electron donor in solution).

confirmed the photoactivity of the Pyr chromophore in both the 1:1 A8Pyr/SSA4WA and 1:1 A8Pyr/SSA6 SAMs (Figure 8(B)). However, the photocurrents measured for the latter SAMs were definitely less intense than those measured in the case of peptides functionalized with the Pyr chromophore, but covalently linked to the gold surface through the lipo group. To investigate in more detail the role of the peptide–gold interface in determining the efficiency of the ET process, the dependence of the anodic photocurrent on the applied potential was analyzed at the Pyr maximum excitation wavelength (λ = 340 nm) for the SSA6Pyr and the A8Pyr/SSA4WA peptide SAMs (Figure 9). The same analysis was also carried out for the SSA6 SAM as a control and background experiment.

In all cases, a decrease in the anodic photocurrent intensity was observed upon reducing the positive bias voltage to the working electrode, and a null photocurrent was measured at a characteristic potential (zero-current potential). This result is due to the fact that the less positive the applied bias, the smaller is the energy gap between the oxidation potentials of the excited Pyr and the gold electrode Fermi level, i.e. the ET driving force in the normal Marcus region. The slope of the photocurrent/voltage curve depends on the electronic coupling between the antenna chromophore and the density of the metal electronic states across the peptide bridge, i.e. the tunneling matrix H_{AD} [47]. The observed linear dependence of the generated photocurrent on the applied potential emphasizes the role of the peptide matrix in the ET process, but it does not allow *per se* to distinguish between a coherent tunneling super-exchange and a diffusive hopping mechanism, because both ET models were shown to be linearly dependent on the applied potential at low voltages [47]. The photocurrent/voltage measurements reported in Figure 9 show that the slope of the P/V curve for the SSA6Pyr SAM is definitely steeper than that measured for the A8Pyr/SSA4WA SAM. This finding may be ascribed to the different types of interaction established by the two SAMs at the peptide–gold interface (junction effect). The $Au^{\delta+}$–$S^{\delta-}$ junction, an almost chemical bond ($\approx$40 kcal·mol^{-1}) with a strong polar character (positive end at the gold surface), allows for a through-bond ET pathway, with a relatively low ET activation barrier at the gold–peptide interface. This pathway cannot be operative for A8Pyr, which lacks the disulfide group and is firmly embedded into the bi-component SAM by favorable interchain interactions with SSA4WA or SSA6. In the latter case, a direct Pyr* → Au ET across the A8Pyr peptide chain would necessarily require a through-space step from the peptide N-terminus to the gold surface, which demands a very

for the SSA6 SAM, also shown in Figure 8(A). In this case, the measured photocurrent may be ascribed to a photothermal effect, i.e. a potential drop caused by heating of the diffusion layer at the electrode interface upon illumination, recently discussed by Kraatz and coworkers [46]. It should be noted that the ratio of the photocurrent intensities of SSA6Pyr and 1:10 SSA6Pyr/SSA6 does not parallel, within experimental errors, the nominal ratio of the Pyr-functionalized peptide content in the deposition solutions. This effect could be obviously ascribed to a different SSA6Pyr/SSA6 ratio in the supported SAM with respect to the deposition solution. Alternatively, the excited-state interaction (excimer formation) in the SSA6Pyr SAM, revealed by fluorescence measurements, could decrease the photocurrent generation efficiency by opening new Pyr–Pyr relaxation channels. This point will be the subject of future investigation.

It is important to stress that in all cases the peptide SAMs covalently linked to the gold surface *via* Au–S interactions were very stable and allowed to reversibly carry out the photocurrent experiments for a full day (at the low applied potentials of experiments) without any damage to the surface coverage. The observation of an anodic photocurrent in the TEOA solution and a photocurrent action spectrum identical to those measured for the SSA6Pyr and 1:10 SSA6Pyr/SSA6 SAMs

Figure 8. Photocurrent action spectra in the Pyr absorption region of gold electrodes modified by: (A) SSA6Pyr (full line), 1:10 SSA6Pyr/SSA6 (dotted line) and SSA6 (dashed line) SAMs, and (B) 1:1 A8Pyr/SSA4WA (dashed line) and 1:1 A8Pyr/SSA6 (full line) SAMs. Applied potential: 0V *versus* Ag/AgCl in all cases. The spectra were normalized by the electrode geometric surface and by the exciting source intensity.
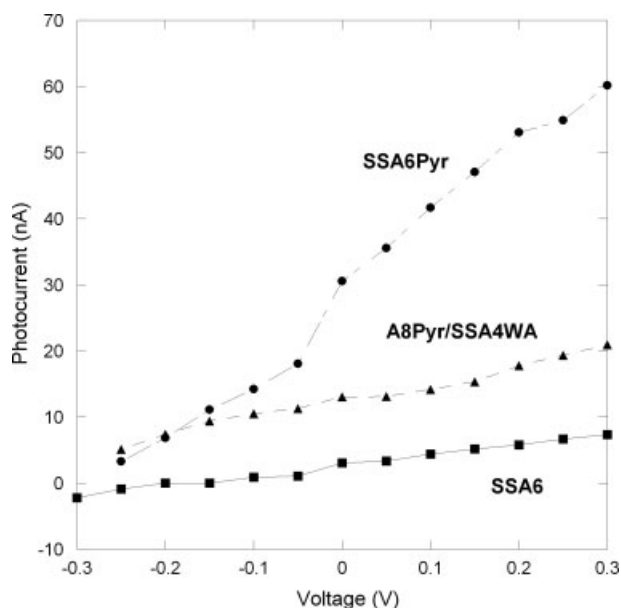
Figure 9. Photocurrent generated by SSA6Pyr (full circles), A8Pyr/SSA4WA (full triangles) or SSA6 (full squares) peptide SAMs by excitation at 340 nm as a function of the applied bias potential. The slope of the reported curves is proportional to the electronic coupling between the electron donor and the electrode density of states, mediated by the peptide chain.

high-barrier activation energy. Furthermore, the A8Pyr helix dipole moment directed in the bi-component SAM with the negative end pointing toward the gold electrode would definitely hinder an ET process in that direction. A possible alternative pathway may proceed through an initial intermolecular ET step from the excited Pyr to the Trp group (Pyr* + W → Pyr$^{+\bullet}$ + W$^-$) or to the –CONH– site of a nearby peptide chain, followed by ET across the Au–S-linked peptide chain from the Trp or the peptide radical to the gold surface. This second step should be also favored by the electrostatic field generated by the peptide helix. Interestingly, the IPCE of the A8Pyr/SSA4WA SAM (IPCE = 0.02%) is definitely greater than the one measured for the A8Pyr/SSA6 SAM (ICPE = 0.006%), suggesting a predominant contribution of the Trp group to the interchain ET process with respect to the amide sites. In any case, the photocurrents generated by the A8Pyr/SSA4WA and A8Pyr/SSA6 SAMs are definitely greater than that measured for the SSA6 SAM (IPCE = 0.002), emphasizing once more the role of Pyr as an antenna chromophore even in the case of a peptide not covalently linked to the gold surface.

Conclusions

Mono- and bi-component SAMs formed by peptide foldamers and covalently linked on gold surfaces were investigated by spectroscopic and electrochemical methods. We conclude that these systems could represent simple and well-defined models for studying heterogeneous electron transfer processes. This result was made possible for the particular nature of the peptides investigated, able to attain helically ordered conformations despite the shortness of their main chain. This property, in turn, is due to the unique conformational properties of their amino acid components, i.e. the C^α-tetrasubstituted residues. These helical peptides were thus shown to be able to give rise to stable and densely packed SAMs and to generate reversible electronic currents under

continuous illumination with good efficiency. A further important consequence of the helical structure of the peptide components is associated with their electrostatic properties, which, giving rise to SAMs endowed with a specific polarity, strongly affects the efficiency and the pathway of the ET process.

In particular, we have shown that it is possible: (i) to modulate the photoactive wavelength region and the efficiency of the ET process by functionalizing the peptide scaffold with a suitable chromophore (*antenna effect*), (ii) to form bi-component peptide SAMs by exploiting favorable interchain interactions, (iii) to open additional ET pathways, promoted by lateral interchain interactions in bi-component SAMs and (iv) to tune the coupling between the photoactive layer and a conductive substrate by changing the nature of the interface (covalently linked or physically adsorbed) embedding the electron donor states (*junction effect*). These findings could be of remarkable importance for the design of new bioinspired materials for nanoelectronics and optoelectronic devices based on conductive organic thin films.

Supporting information

Supporting information may be found in the online version of this article.

References

1 Lehn J-M. Toward complex matter: supramolecular chemistry and self-organization. *PNAS* 2002; **99**: 4673–4678.
2 Love JC, Estroff LA, Kriebel JK, Nuzzo RG, Whitesides GM. Self-assembled monolayers of thiolates on metals as a form of nanotechnology. *Chem. Rev.* 2005; **105**: 1103–1170.
3 Stupp SF. Introduction: functional nanostructures. *Chem. Rev.* 2005; **105**: 1023–1024.
4 Langer R, Tirrell DA. Designing materials for biology and medicine. *Nature* 2004; **428**: 487–492.
5 Zhang S. Fabrication of novel materials through molecular self-assembly. *Nat. Biotechnol.* 2003; **21**: 1171–1178.
6 Fendler JH. Chemical self-assembly for electronic applications. *Chem. Mater.* 2001; **13**: 3196–3210.
7 Seelig G, Soloveichik D, Zhang DY, Winfree E. Enzyme-free nucleic acid logic circuits. *Science* 2006; **314**: 1585–1588.
8 Xia Y, Rogers JA, Paul KE, Whitesides GM. Unconventional methods for fabricating and patterning nanostructures. *Chem. Rev.* 1999; **99**: 1823–1848.
9 Willner I, Katz E. *Bioelectronics: from Theory to Applications*. Wiley-VCH: Weinheim, Germany, 2005.
10 Gellman SH. Foldamers: a manifesto. *Acc. Chem. Res.* 1998; **31**: 173–180.
11 Toniolo C, Crisma M, Formaggio F, Peggion C. Control of peptide conformation by the Thorpe-Ingold effect (*C*-alpha tetrasubstitution). *Biopolymers (Pept. Sci.)* 2001; **60**: 396–419.
12 Karle IL, Balaram P. Structural characteristics of alpha-helical peptide molecules containing Aib residues. *Biochemistry* 1990; **29**: 6747–6756.
13 Toniolo C, Benedetti E. The polypeptide 3₁₀-helix. *Trends Biochem. Sci.* 1991; **16**: 350–353.
14 Long YT, Abu-Irhayem E, Kraatz HB. Peptide electron transfer: more questions than answers. *Chem. Eur. J.* 2005; **11**: 5186–5194.

15 Antonello S, Formaggio F, Moretto A, Toniolo C, Maran F. Anomalous distance dependence of electron transfer across peptide bridges. *J. Am. Chem. Soc.* 2003; **125**: 2874–2875.

16 Morita T, Kimura S, Kobayashi S, Imanishi Y. Photocurrent generation under a large dipole moment formed by self-assembled monolayers of helical peptides having an *N*-ethylcarbazolyl group. *J. Am. Chem. Soc.* 2000; **122**: 2850–2859.

17 Shin YK, Newton MD, Isied SS. Distance dependence of electron transfer across peptides with different secondary structures: the role of peptide energetic and electronic coupling. *J. Am. Chem. Soc.* 2003; **125**: 3722–3732.

18 Galoppini E, Fox MA. Effect of the electric field generated by the helix dipole on photoinduced intramolecular electron transfer in dichromophoric α-helical peptides. *J. Am. Chem. Soc.* 1996; **118**: 2299–2300.

19 Fox MA, Galoppini E. Electric field effects on the electron transfer rates in dichromophoric peptides: the effect of helix unfolding. *J. Am. Chem. Soc.* 1997; **119**: 5277–5285.

20 Gatto E, Porchetta A, Stella L, Guryanov I, Formaggio F, Toniolo C, Kaptein B, Broxterman QB, Venanzi M. Conformational effects on the electron transfer efficiency in peptide foldamers based on α,α-disubstituted glycyl resides. *Chem. Biodivers.* 2008; **5**: 1263–1278.

21 Venanzi M, Pace G, Palleschi A, Stella L, Castrucci P, Scarselli M, De Crescenzi M, Formaggio F, Toniolo C, Marletta G. Densely-packed self-assembled monolayers on gold surfaces from a conformationally constrained helical hexapeptide. *Surf. Sci.* 2006; **600**: 409–416.

22 Pace G, Venanzi M, Castrucci P, Scarselli M, De Crescenzi M, Palleschi A, Stella L, Formaggio F, Toniolo C, Marletta G. Static and dynamic features of a helical hexapeptide chemisorbed on a gold surface. *Mater. Sci. Eng. C* 2006; **26**: 918–923.

23 Wen X, Linton RW, Formaggio F, Toniolo C, Samulski ET. Self-assembled monolayers of hexapeptides on gold: surface characterization and orientation distribution analysis. *J. Phys. Chem. A* 2004; **108**: 9673–9681.

24 Gatto E, Stella L, Formaggio F, Toniolo C, Lorenzelli L, Venanzi M. Electroconductive and photocurrent generation properties of self-assembled monolayers formed by functionalized, conformationally-constrained peptides on gold electrodes. *J. Pept. Sci.* 2008; **14**: 184–191.

25 Birks JB. *Photophysics of Aromatic Molecules*. Wiley: New York, NY, 1970.

26 Gatto E, Stella L, Baldini C, Toniolo C, Formaggio F, Venanzi M. Photocurrent generation in peptide-based self-assembled monolayers on gold electrodes. *Superlattices Microstruct.* 2009; **46**: 34–39.

27 Baldini C. Synthesis and conformational characterization, Ph. D. Thesis, University of Padova, 2007.

28 Kakiuchi T, Usui H, Hobara D, Yamamoto M. Voltammetric properties of the reductive desorption of alkanethiol self-assembled monolayers from a metal surface. *Langmuir* 2002; **18**: 5231–5238.

29 Khazraji AC, Hotchandani S, Das S, Kamat PV. Controlling dye (Merocyanine-540) aggregation on nanostructured TiO_2 films. An organized assembly approach for enhancing the efficiency of photosensitization. *J. Phys. Chem. B* 1999; **103**: 4693–4700.

30 Kuhn JH, Braslavsky SE, Schmidt R. Chemical actinometry. *Pure Appl. Chem.* 1989; **61**: 187–210.

31 Burla MC, Camalli M, Carrozzini B, Cascarano GL, Giacovazzo C, Polidori G, Spagna R. SIR2002: the program. *J. Appl. Crystallogr.* 2003; **36**: 1103.

32 Sheldrick GM. A short history of SHELX. *Acta Crystallogr. A* 2008; **64**: 112–122.

33 Toniolo C, Polese A, Formaggio F, Crisma M, Kamphuis J. Circular dichroism spectrum of a peptide 3_{10}-helix. *J. Am. Chem. Soc.* 1996; **118**: 2744–2745.

34 Fujita K, Bunjes N, Nakajima K, Hara M, Sasabe H, Knoll M. Macrodipole interaction of helical peptides in a self-assembled monolayer on gold substrate. *Langmuir* 1998; **14**: 6167–6172.

35 Flink S, Van Veggel FCJM, Reinhoudt DN. Functionalization of self-assembled monolayers on glass and oxidized silicon wafers by surface reactions. *J. Phys. Org. Chem.* 2001; **14**: 407–415.

36 Nakamura M, Saito N, Takayama K, Kumamoto S, Yamana K. Highly emissive pyrene-excimer formation in self-assembled monolayers on gold surface and photocurrent generation from the excimer. *Chem. Lett.* 2007; **36**: 602–603.

37 Polo F, Antonello S, Formaggio F, Toniolo C, Maran F. Evidence against the hopping mechanism as an important electron transfer pathway for conformationally constrained oligopeptides. *J. Am. Chem. Soc.* 2005; **127**: 492–493.

38 Cordes M, Köttgen A, Jasper C, Jacques O, Boudebous H, Giese B. Influence of amino acid side chains on long-distance electron transfer in peptides: electron hopping via "stepping stones". *Angew. Chem. Int. Ed.* 2008; **47**: 3461–3463.

39 Malak RB, Gao Z, Wishart JF, Isied S. Long-range electron transfer across peptide bridges: the transition from electron super-exchange to hopping. *J. Am. Chem. Soc.* 2004; **126**: 13888–13889.

40 Morita T, Kimura S, Kobayashi S, Imanishi Y. Photocurrent generation by the self-assembled monolayers integrating a photoenergy-harvesting system and an electron-transport system of helical peptide. *Chem. Lett.* 2000; **29**: 676–677.

41 Yasutomi S, Morita T, Imanishi Y, Kimura S. A molecular photodiode system that can switch photocurrent direction. *Science* 2004; **304**: 1944–1947.

42 Yanagisawa K, Morita T, Kimura S. Efficient photocurrent generation by self-assembled monolayers composed of 3_{10}-helical peptides carrying linearly spaced naphthyl groups at the side chains. *J. Am. Chem. Soc.* 2004; **126**: 12780–12781.

43 Yasutomi S, Morita T, Kimura S. pH-controlled switching of photocurrent direction by self-assembled monolayers of helical peptides. *J. Am. Chem. Soc.* 2005; **127**: 14564–14565.

44 Morita T, Yanagisawa K, Kimura S. Enhanced photocurrent generation by electron hopping through regularly-arranged chromophores in a helical peptide monolayer. *Polym. J.* 2008; **40**: 700–709.

45 Okamoto S, Morita T, Kimura S. Photocurrent generation by self-assembled monolayers of helical peptides carrying naphthyl groups and ferrocene unit as hopping sites. *Chem. Lett.* 2009; **38**: 126–127.

46 Mandal HS, Burgess IJ, Kraatz HB. Investigation of laser induced photocurrent generation experiments. *Chem. Commun.* 2006; 4802–4804.

47 McCreery RL. Molecular electronic junctions. *Chem. Mater.* 2004; **16**: 4477–4496.